Research article

Basudeb Sain[a], Roy Kaner[a], Yaara Bondy and Yehiam Prior*

Plasmonic flat surface Fabry-Perot interferometry

https://doi.org/10.1515/nanoph-2017-0082
Received August 29, 2017; revised October 13, 2017; accepted November 14, 2017

Abstract: We report measurements of the optical transmission through a plasmonic flat surface interferometer. The transmission spectrum shows Fabry-Perot-like modes, where for each mode order, the maximal transmission occurs at a gap that grows linearly with wavelength, giving the appearance of diagonal dependence on gap and wavelength. The experimental results are supported by numerical solutions of the wave equations and by a simplified theoretical model that is based on the coupling between localized and propagating surface plasmon. This work explains not only the appearance of the modes but also their sharp dependence on the gap, taking into consideration the refractive indices of the surrounding media. The transmission spectra provide information about the phase difference between the light impinging on the two cavities, enabling interferometric measurement of the light phase by transmission through the coupled plasmonic cavities. The 1° phase-difference resolution is obtained without any propagation distance, thus making this interferometer suitable for on-chip operation.

Keywords: plasmonics; surface plasmons; optical transmission; Fabry-Perot interferometer.

1 Introduction

A perforated metal film is not just a screen that blocks light. The extraordinary optical transmission through a film containing subwavelength apertures was shown to be much higher than would be expected by the classical Bethe small-hole-diffraction-theory [1]. It is the collective response of surface plasmons in the metallic film that boosts the transmission [2–6]. There has been a surge of research related to plasmon-mediated optical transmission through multiple cavities in metal films, be it simple combinations of two slits or more complicated interacting arrays, where the shape of each cavity and the gaps between them determine the optical response of the complex nanostructures [7–13].

The interaction between two nanoparticles or two nanocavities in a metal film is a fundamental route by which plasmon-plasmon interactions create new electromagnetic modes, leading to the manipulation of light on a subwavelength scale. A number of studies have been reported on the optical response of pairs of nanostructures with varying gaps between them. Due to the rapid evanescent decay of the field at the metal-air interface, metallic nano-particle dimers demonstrate a very short range (tens of nanometers) of interaction between them [14, 15]. Nanocavities in metallic films, on the other hand, have a much larger interaction range. For properly polarized input beams [8, 16], the localized plasmons excited in each cavity interact via propagating surface plasmon polaritons (SPPs), and the range of interaction is the range of plasmonic propagation decay which can be large (many microns).

Far-field spectra displaying strong dependence on the gap between slits were presented by Schouten et al. [9], where the double-slit interference pattern was explained in terms of the interaction between the propagation of SPPs through the two slits. Zhi et al. [13] studied plasmon-assisted transmission in two kinds of slit structures in a silver film on a glass substrate. They observed that when one of the two slits was replaced by a shallow corrugation, the transmission spectra displayed a simple sinusoidal intensity modulation, but when two open slits were used, a more complex transmission spectrum resulted. These authors attributed their observations to different propagation constants of the SPPs at the silver-air and silver-glass interfaces. Lalanne et al. [10] observed transmission modes with dependence on the plasmonic wavelength and the gap between the cavities. The observation of constructive interference for integer multiples of the plasmonic wavelength was reported by Janssen et al. [17]. Chen et al. [18] simulated transmission spectra of slit-groove configuration in silver and in perfect electrical conductor; at short gap distances, they observed a modulation resulting not

[a]**Basudeb Sain and Roy Kaner:** These authors contributed equally to this work.
***Corresponding author: Yehiam Prior,** Department of Chemical Physics, Weizmann Institute of Science, Rehovot 76100, Israel, e-mail: yehiam.prior@weizmann.ac.il
Basudeb Sain, Roy Kaner and Yaara Bondy: Department of Chemical Physics, Weizmann Institute of Science, Rehovot 76100, Israel

only from the surface plasmons but also from interference between the incident light and the radiation generated by the scattering at the groove.

Here we study the effect of both propagating and localized surface plasmons (LSP) in optical transmission through plasmonic double-slit flat surface interferometer and observe the appearance of diagonal modes (positioned diagonally as a function of the gap). In our simplified theoretical model we included, for the first time to our knowledge, the contribution of LSP and more importantly, the effect of propagating SPP reflection from the cavities. The experimental results are further supported by a numerical solution of the wave equation.

2 Materials and methods

The gold films of typical thickness 200 nm were e-beam evaporated on 0.3 mm thick clean borosilicate glass of 18×18 mm^2 (Waldemar Knittel Glasberbeitungs GmbH), with deposition rate of around 0.05 nm/s. In order to achieve high signal to noise ratio, two-dimensional arrays, consisting of 100 pairs (10×10) of rectangular cavities of dimension 100 [nm] $\times$ 800 [nm], separated by various gaps that varied from 100 nm to 3100 nm in steps of 50 nm, were milled using focused ion beam microscope (FEI, Helios Nano Lab 600i) with a Ga ion and electron source, into high quality gold films (Figure 1). The gap remained constant for all the pairs in each array. A 10 μm distance was maintained between two closest pairs in both directions for all the arrays to avoid any plasmonic interaction.

The transmission spectrum was measured using Nanonics Dual Microscope Combined Upright and Inverted Systems (Nanonics MV4000). An objective (Nikon LU Plan Fluor 10X/0.30) was used to mildly focus white light from a halogen lamp (Osram HLX 64623) on the sample from below. The light was polarized linearly by a cubic beam-splitter placed between the light source and the objective. The transmitted signal from the region of interest (from each array) was collected using a high magnification objective (Nikon TU Plan Fluor 100X/0.90) from above. Additional iris was put after the collection objective to decrease the background noise. The transmitted spectrum was measured by Renishaw inVia Raman Spectrometer.

The far-field optical transmission was calculated by the finite-difference time-domain (FDTD) method using the commercial software Lumerical FDTD Solutions. We simulated a pair of rectangular nanocavities of dimension 100 [nm] $\times$ 800 [nm], separated by various gaps that varies from 100 nm to 3100 nm in steps of 50 nm. In all the simulations, the dimensions of the mesh around the nanocavities were set to $dx = dy = dz = 5$ nm, and perfectly matched layers were added in all dimensions to avoid reflections. The optical constants of Au were extracted from the Johnson and Christy tables, while the optical constants of SiO_2 were taken from Palik. The light source was a plane wave linearly polarized along the line joining the pair of cavities, travelling in a direction perpendicular to the plane of the cavities. A frequency-domain field and power monitor was placed on top of the gold film to capture the far-field transmission.

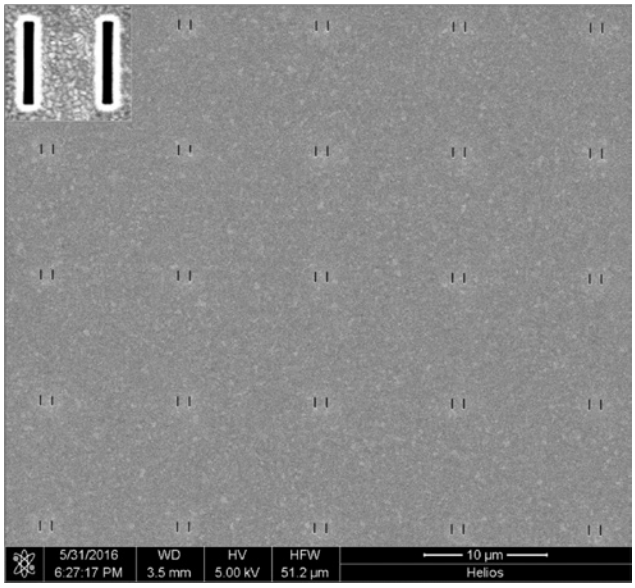

Figure 1: Fabricated sample for measurements.
Magnified SEM image (partial view) of a two-dimensional array consisting of 100 pairs of rectangular cavities of dimension 100 [nm] $\times$ 800 [nm] in 10×10 matrix format. The cavities were milled in a high-quality gold film of thickness 200 nm. The inset shows a typical image (magnified) of a pair of nanocavities.

A simplified model has been developed to explain the experimental and simulation results. The model is based on the interaction between LSP and SPPs at the different gaps and the refractive indices surrounding and inside each cavity.

3 Results and discussion

For a single nanocavity, the enhancement of the transmission is caused by a localized plasmonic resonance. Excitation of the cavity by light gives rise to LSPs in and around the cavity, which in turn create near-field electromagnetic radiation that interferes with the incoming beam and

enhances the transmission through the hole [19]. The resonance peak depends on the film metal, the surrounding materials, and cavity geometry [20]. For coupled cavities, the situation is different: the LSPs couple to the SPPs which are generated at the cavity edges. The direction of propagation of the SPPs is dictated by the polarization axis, in our case, the line connecting the pair of neighboring cavities. Clearly, SPPs propagate also to other directions away from the neighboring hole, but this decaying evanescent field does not contribute to the transmitted light. When the SPP reaches the neighboring cavity, some of its energy couples to an LSP in that cavity, resulting in an enhancement or suppression of the already existing LSP depending on the relative phase between them. The remaining part of the energy is reflected back such that the two cavities form a unique Fabry-Perot (F-P) interferometer for the propagating plasmonic surface waves. In this F-P interferometer, the plasmons propagate in the interface, and their interference affects the transmission of light through the structure. Thus, this is a flat interferometer (Figure 2), where phase is accumulated in a plane perpendicular to the propagation direction. In what follows, we analyze this interference of the propagating plasmons theoretically and present numerical simulations for the transmitted light intensity.

Consider the transmission through a double-cavity configuration, with the observation that the transmission through the bare gold film is negligible. The light transmitted through the sample is the result of a plasmonic near field converted to the far field; thus, we calculate the field near the surface around the two cavities, and the transmitted light is expected to be proportional to this quantity.

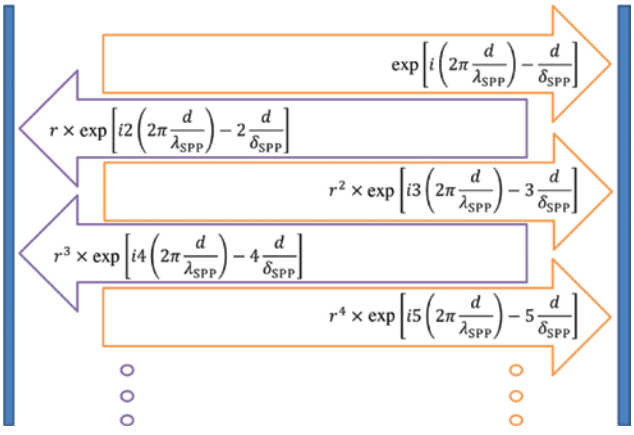

Figure 2: Plasmonic Fabry-Perot flat interferometer.
Upon excitation of localized plasmons on both sides, the SPPs propagate from one cavity to the other, accumulate phase and are reflected, giving rise to two infinite geometric series leading to the transmitted intensity.

A LSP is excited by the incoming light and then couples to a surface plasmon which propagates away in both directions (we consider only propagation along the line connecting the two cavities). As a function of x, the distance away from the cavity, the intensity of the SPP accumulates a phase factor and is given by

$$E_{SPP}(x)=\alpha\times\beta\times\exp\left[i\left(2\pi\frac{d}{\lambda_{SPP}}\right)\right]\times\exp\left(-\frac{x}{\delta_{SPP}(\lambda)}\right), \quad (1)$$

where α is the coupling coefficient between the incoming radiation and the excited LSP, and β is the coupling coefficient between excited LSPs and propagating SPPs. Both α and β are, in principle, wavelength dependent. λ_{SPP} is the plasmonic wavelength, and δ_{SPP} is the plasmon propagation decay length [21]. While α is a general proportionality constant defining the efficiency of the excitation, β is a more important factor, controlling the ratio between the contributions of the LSP and the SPP, respectively. Once the SPP reaches the second cavity, part of it is converted back to LSP with the same coefficient β, and part of it is reflected back with a coefficient 'r'. Here, we assumed 'r' to be real and wavelength independent. The SPP is reflected back towards the first cavity and accumulates the same phase factor, in a manner completely equivalent to optical F-P. Naturally, the same analysis applies to an LSP excited originally at the second cavity. Thus, the total near field for two cavities positioned a distance 'd' apart and excited simultaneously is given by the sum of two geometric series:

$$E_{total}(d)\sim\frac{\exp(i2\pi d/\lambda_{SPP}-d/\delta_{SPP})}{1-r^2\times\exp[(i2\pi d/\lambda_{SPP})-d/\delta_{SPP}]}. \quad (2)$$

The transmission is proportional to the square of the total local electric field within this interferometer. The periodic function at the denominator gives rise to modes as a function of the distance, d, between the cavities. Qualitatively, as in any F-P interferometer, when the optical path is an integer multiple of the wavelength, constructive interference occurs, which in the present case happens when

$$d=\lambda_{SPP}\times n, \quad (n\in\mathbb{N}). \quad (3)$$

Independent of the F-P model calculation, the transmitted spectrum can be directly calculated by solving the wave equation numerically. We use the FDTD method implemented on the Lumerical software package (details are in Section 2), for various configurations and material composition.

In Figure 3 the calculated transmission is plotted for the F-P model and compared to prediction of the direct numerical simulations for several configurations. In the

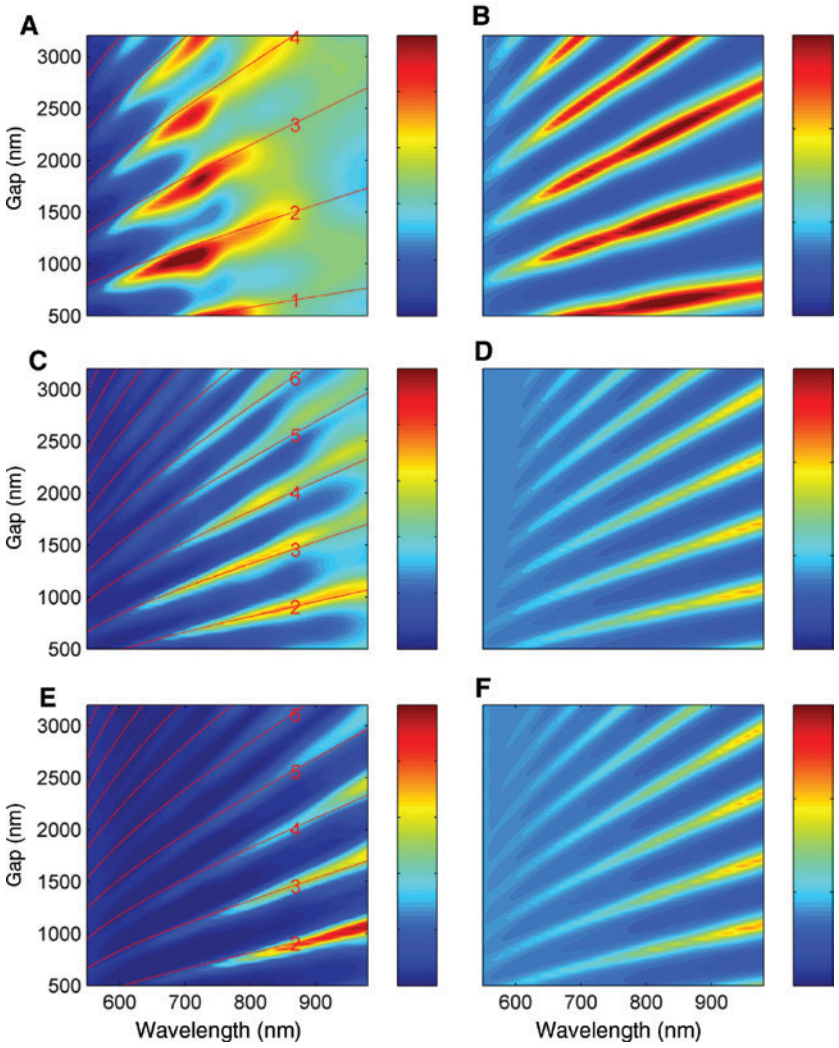

Figure 3: Transmission results from various configurations and material composition.
Simulated (left) and calculated (right) transmission spectra for three different configurations of cavities of dimension 100×800 nm milled in a 200 nm thick gold film; (A) and (B) free-standing film, (C) and (D) gold on glass and (E) and (F) a gold film surrounded by glass on both sides. In the model, the parameters used were for $\beta = 0.2$ and $r = 0.6$. The optical constants of gold were taken from Johnson and Christy tables [22], and the data for the SiO_2 were taken from Palik [23]. The calculated mode frequencies are plotted as red lines, on top of the simulation results.

model, the values of the reflection coefficient 'r' and 'β' were fitted for best visual overlap with the numerical results; based on the quality of the experimental data, we did not perform any further numerical analysis for a more accurate derivation of these parameters. The model agrees well with the numerical simulation results by predicting the appearance, location, and spacing of the modes and the location of the peak of each mode. In order to further emphasize the agreement between model and the simulation results, the calculated mode frequencies are plotted on top of the simulation results (red lines).

The simplified F-P model captures the main features of the diagonal modes, but it does not cover the entire physical situation. The model is based on a single plasmonic wavelength, which may be valid if the gold film is surrounded by a single medium (i.e. air or glass), but when the different sides are made of different materials, the plasmonic frequencies are different on the different sides [24]. For the mixed material case we find that one of the modes is dominant, and we use that mode. Thus, for the mixed glass air case, the gold glass interface determines the F-P behavior and was used in our modelling.

In the experiments, pairs of rectangular cavities with varying gaps were milled into 200 nm thick gold film, deposited on glass. The sample preparation and

experimental methodology are described in Section 2. Each array was illuminated from the glass side by linearly polarized white light from a halogen lamp. The polarization direction was set to be along the line joining the pair of the cavities. The transmitted signal was collected in two separate measurements: (1) the illumination is from the glass side and measurement from the air side and (2) the illumination is from the glass side, but on the air side, a layer of poly(methyl methacrylate) was deposited on the gold film, so that the refractive index was matched at ~1.5 on both sides.

Figure 4 depicts the experimental results, shown in a single spectrogram for each configuration. The left columns (Figure 4A and C) present the raw data as measured, whereas the right columns (Figure 4B and D) present the normalized data. The data were normalized by the input white light intensity and by the sum total of the observations over all gaps in order to also take into consideration the wavelength-dependent transmission of the gold film. The red lines (from the model) are mostly overlapped with the position of the modes in both measurements. Previously, we have seen that there is good agreement between simulation and model (Figure 3). Typically, the numerical simulations predict the qualitative nature of the physical observations, but they cannot be expected to yield quantitative agreement with the measured results. The dimensions of the fabricated cavities are not exactly as designed; the sharpness of the facets and corners is not perfect (as is assumed in the simulations), surface imperfections are not accounted for, metal grains and layer thickness fluctuations are ignored, and several other such "technical" imperfections are found to affect the details of the simulated results. The general agreement of the results obtained from measurements, simulations, and model calculations gives credence to the assumptions used to develop the model.

Note that a small constant shift seems to appear between the model-calculated and numerically simulated (or measured) mode positions: 180 nm and 280 nm, respectively. This shift may result from the thickness of the layer, where the plasmons are not reflected from the edge but also penetrate the hole or from constant phase added to the SPPs with each reflection. These effects were not included in the current model, and further work is needed to fully interpret these observations.

A regular F-P interferometer operates longitudinally, namely, the interference is along the propagation direction, and thus its operation requires some propagation

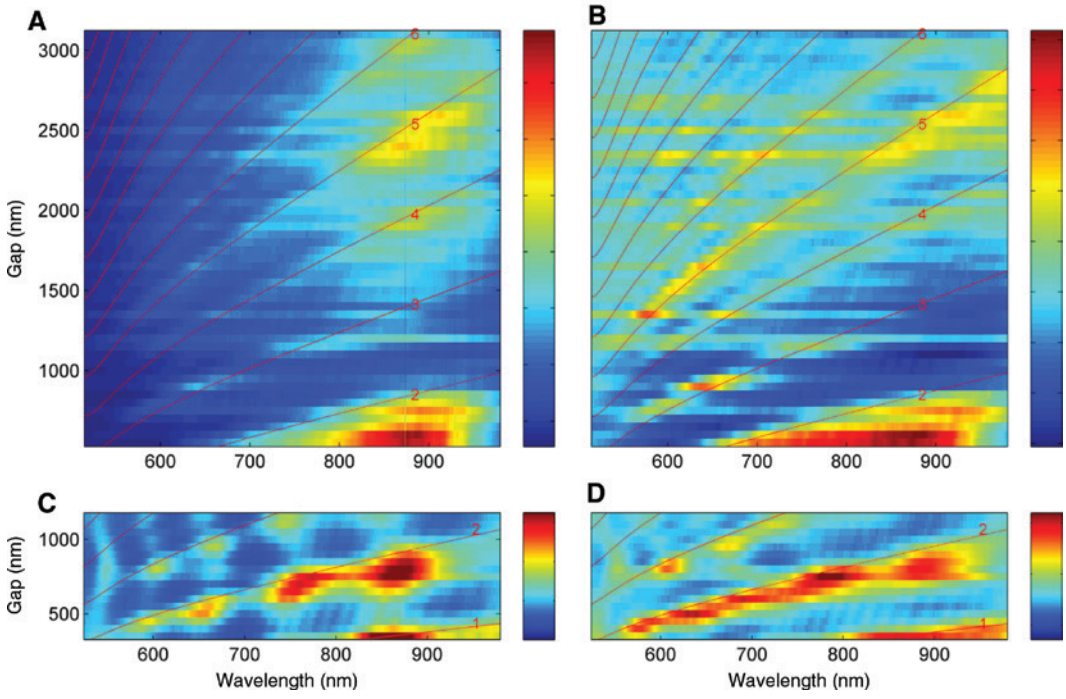

Figure 4: Measured transmission with different normalization.
Transmission spectra for glass-air-air and glass-glass-glass combinations. (A) Gold film on glass with air above the film (air-glass), (B) normalized air-glass, (C) glass-glass modes and (D) normalized glass-glass. All data were normalized by the white light spectrum, and the right column was also normalized to the sum total of the average intensity measured for all gaps. Due to the rapid decay of the modes in the case of glass-glass, only smaller gaps are shown. The calculated mode frequencies are included as red lines.

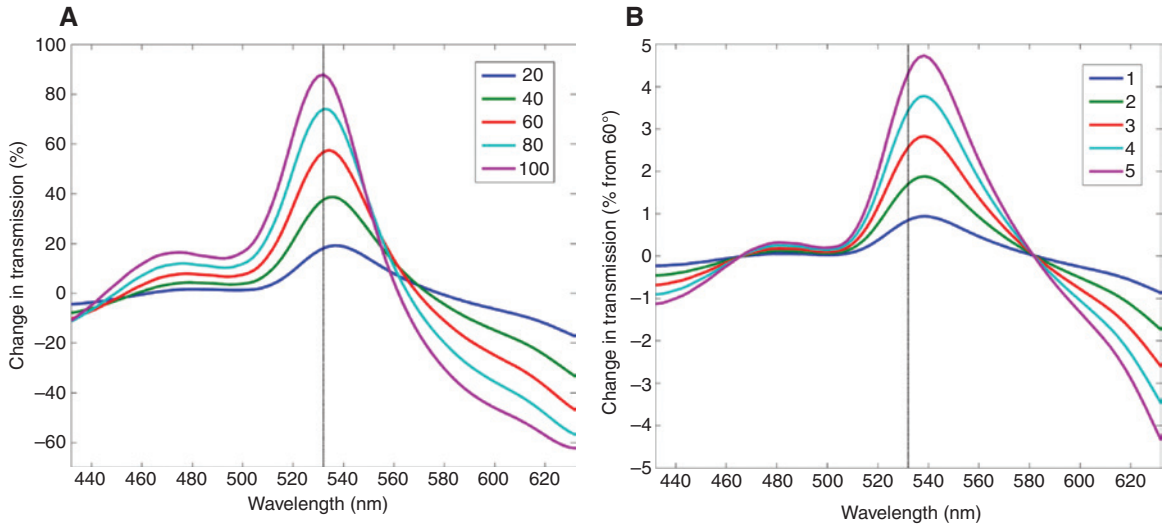

Figure 5: Flat interferometer.
Change in transmission spectra of two holes separated by 1.3 μm, illuminated by two separate beams with a fixed delay between them. The phase difference at 532 nm is shown by the different colors in the inset (A) phase change over a large range of 0–100°, (B) smaller range of 0–5°. From part (B) one can deduce that the phase resolution for a 1% amplitude noise is approximately 1°.

length. The current plasmonic interferometer is different – it operates in a plane perpendicular to the propagation direction. This difference in geometry makes the current interferometer suitable for on-chip operation. In what follows we present a numerical simulation that demonstrates the feasibility of phase-difference resolution of this interferometer. For realistic applications at a given wavelength, the gap between the cavities will have to be selected and the expected phase-difference resolution estimated for the specific set of parameters. For a given gap between two cavities we illuminated each cavity by a separate beam and numerically introduce a phase difference between them. A detector was placed above one of the cavities to capture transmission through that cavity. Figure 5 depicts the change in transmission (as measured by the numerical detector) of two holes separated by a distance of 1.3 μm, illuminated separately with two beams with a fixed delay between them. The gap of 1.3 μm was chosen for a maximal difference at 532 nm, and the phase differences at this wavelength are shown in the inset. Based on the large variation in the transmission as a function of the phase difference, interferometry can be performed with near-zero propagation length along the original direction of the beams, suitable for on-chip operation. To estimate the potential phase resolution of such an interferometer, Figure 5B depicts the changes for small phase variations of 1°–5°. Clearly, the laser noise will determine the phase-difference resolution, and for a reasonable amplitude noise of 1%, we can expect phase resolution of approximately 1°.

4 Conclusion

In conclusion, the far field optical transmission through pairs of coupled nanocavities with different gaps has been measured in different configurations. Well-defined diagonal transmission modes are observed in a single spectrogram. The experimental results are supported by a numerical solution of the wave equation and by a simplified theoretical model that is based on the interaction between localized and propagating surface plasmons at different gaps. In this configuration, two beams impinge on a flat metal layer with two cavities milled into it, and the intensity is measured over one of the cavities. The 1° phase resolution is obtained without any longitudinal propagation of the light. This configuration of two coupled cavities is proposed as a planar interferometer suitable for on-chip operation. Based on the sharp dependence of wavelength, one may envisage applications where spectral selectivity is needed. Bulk spectrometers necessarily reduce the light throughput and thus reducing sensitivity, and the present device may find applications for high sensitivity Raman measurements. Furthermore, the flatness of the device may be useful for detection arrangements where small size is required. Further work is under way to probe these options.

Acknowledgments: Useful discussions with Euclides Almeida and Guy Shalem are gratefully acknowledged. This work was supported by the Israel Science Foundation grant no. 1242/12, by the ICORE program, by an FTA

grant from the Israel National Nano Initiative and by the Minerva Foundation.

References

[1] Ebbesen TW, Lezec HJ, Ghaemi HF, Thio T, Wolff PA. Extraordinary optical transmission through sub-wavelength hole arrays. Nature 1998;391:667–9.
[2] Liu HT, Lalanne P. Microscopic theory of the extraordinary optical transmission. Nature 2008;452:728–31.
[3] Martin-Moreno L, Garcia-Vidal FJ, Lezec HJ, et al. Theory of extraordinary optical transmission through subwavelength hole arrays. Phys Rev Lett 2001;86:1114–7.
[4] Selcuk S, Woo K, Tanner DB, Hebard AF, Borisov AG, Shabanov SV. Trapped electromagnetic modes and scaling in the transmittance of perforated metal films. Phys Rev Lett 2006;97:067403.
[5] Hohng SC, Yoon YC, Kim DS, et al. Light emission from the shadows: surface plasmon nano-optics at near and far fields. Appl Phys Lett 2002;81:3239–41.
[6] Chowdhury MH, Lindquist NC, Lesuffleur A, Oh SH, Lakowicz JR, Ray K. Effect of nanohole spacing on the self-imaging phenomenon created by the three-dimensional propagation of light through periodic nanohole arrays. J Phys Chem C 2012;116:19958–67.
[7] Zhang Y, Han M, Huang CP. Plasmon coupling in circular-hole dimers: from separation- to touching-coupling regimes. J Appl Phys 2012;112:013113.
[8] Janipour M, Hodjat-Kashani F. Directional radiation of surface plasmon polaritons at visible wavelengths through a nanohole dimer optical antenna milled in a gold film. J Opt Soc Korea 2014;18:799–808.
[9] Schouten HF, Kuzmin N, Dubois G, et al. Plasmon-assisted two-slit transmission: Young's experiment revisited. Phys Rev Lett 2005;94:053901.
[10] Lalanne P, Hugonin JP, Rodier JC. Theory of surface plasmon generation at nanoslit apertures. Phys Rev Lett 2005;95:263902.
[11] Gordon R, Brolo AG, Sinton D, Kavanagh KL. Resonant optical transmission through hole-arrays in metal films: physics and applications. Laser Photonics Rev 2010;4:311–35.
[12] Kwak ES, Henzie J, Chang SH, Gray SK, Schatz GC, Odom TW. Surface plasmon standing waves in large-area subwavelength hole arrays. Nano Lett 2005;5:1963–7.
[13] Zhi L, Jia-Sen Z, Hai-Feng Y, Qi-Huang G. Complex modulation in plasmon-assisted transmission spectra of a two-slit structure. Chinese Phys Lett 2007;24:3233–6.
[14] Funston AM, Novo C, Davis TJ, Mulvaney P. Plasmon coupling of gold nanorods at short distances and in different geometries. Nano Lett 2009;9:1651–8.
[15] Lassiter JB, Aizpurua J, Hernandez LI, et al. Close encounters between two nanoshells. Nano Lett 2008;8:1212–8.
[16] Salomon A, Prior Y, Fedoruk M, Feldmann J, Kolkowski R, Zyss J. Plasmonic coupling between metallic nanocavities. J Opt 2014;16:114012.
[17] Janssen OTA, Urbach HP, 't Hooft GW. On the phase of plasmons excited by slits in a metal film. Opt Express 2006;14:11823–32.
[18] Chen L, Robinson JT, Lipson M. Role of radiation and surface plasmon polaritons in the optical interactions between a nano-slit and a nano-groove on a metal surface. Opt Express 2006;14:12629–36.
[19] Pardo F, Bouchon P, Haidar R, Pelouard JL. Light funneling mechanism explained by magnetoelectric interference. Phys Rev Lett 2011;107:093902.
[20] Salomon A, Zielinski M, Kolkowski R, Zyss J, Prior Y. Size and shape resonances in second harmonic generation from silver nanocavities. J Phys Chem C 2013;117:22377–82.
[21] Barnes WL. Surface plasmon-polariton length scales: a route to sub-wavelength optics. J Opt A Pure Applied Op 2006;8:S87–93.
[22] Johnson PB, Christy RW. Optical constants of the noble metals. Phys Rev B 1972;6:4370–9.
[23] Palik ED. Handbook of optical constants of solids. San Diego, California: Academic Press, 1998.
[24] Sain B, Kaner R, Prior Y. Phase-controlled propagation of surface plasmons. Light Sci Appl 2017;6:e17072.